Intelligent and Converged Networks ISSN 2708-6240
2022, 3(4): 351−363 DOI: 10.23919/ICN.2022.0029

Enhancing active reconfigurable intelligent surface

Muhammad I. Khalil*

Abstract: A Reconfigurable Intelligent Surface (RIS) panel comprises many independent Reflective Elements (REs). One possible way to implement an RIS is to use a binary passive load impedance connected to an antenna element to achieve the modulation of reflected radio waves. Each RE reflects incoming waves (incident signal) by using on/off modulation between two passive loads and adjusting its phase using a Phase Shifter (PS). However, this modulation process reduces the amplitude of the reflected output signal to less than unity. Therefore, recent RIS works have employed Reflection Amplifiers (RAs) to compensate for the losses incurred during the modulation process. However, these systems only improve the reflection coefficient for a single modulation state, resulting in suboptimal RE efficacy. Thus, this paper proposes a strategy for optimising RE by continuously activating the RA regardless of the switching load state. The performance of the proposed scheme is evaluated in two scenarios: (1) In the first scenario (Sc1), the RA only operates to compensate for high-impedance loads, and (2) in the second scenario (Sc2), the RA runs continuously regardless of the RE loads. To benchmark the performance of Sc1 and Sc2, various metrics are compared, including signal-to-noise ratio, insertion loss, noise figure, communication range, and power-added efficiency. Numerical examples are provided to demonstrate the effectiveness of the proposed scheme. It is found that the proposed system in Sc2 leads to better overall performance compared to Sc1 due to the increased gain of the RIS reflection.

Key words: reflection amplifiers; reflection coefficient; phase-shifter; Reconfigurable Intelligent Surface (RIS)

1 Introduction

Wireless communication capacity has significantly increased over the generations with the development of transceiver designs, while the design of wireless channels has remained uncontrollable. The recent advancement in meta-materials has led to the introduction of Reconfigurable Intelligent Surfaces (RISs) panels, which are capable of intelligently controlling wireless channels to enhance communication performance[1−3]. An RIS panel is an array composed of passive elements that reflect incident signals in the desired way to set the propagation characteristics of a wireless channel[4]. RISs are characterized by high array gain, low power consumption, extended coverage, low cost, and low noise[5−7]. Therefore, RISs are expected to support 5G and future 6G networks with additional envisioned applications, including WiFi extensions, localization improvement, unmanned aerial vehicles, and satellite network extensions[8−11].

An RIS panel comprises significant sub-wavelength Reflecting Elements (REs), which are small antennas such as microstrip patches[12]. Each RE is linked to a tunable chip, such as a PIN diode or varactor diode, to modify its load impedance. One way to implement an RIS is to use a binary on/off modulation diode that changes the load impedance, resulting in a different phase shift. When the diodes are turned on, the incident current flow is slightly hindered by each RE, causing an induction voltage. On the other hand, when the diodes are turned off (open circuit), the impedance load of an RE becomes large, causing little or no induced current to occur. This arrangement allows the reflected

• Muhammad I. Khalil is with the School of Electrical and Electronic Engineering, University of Royal Melbourne Institute of Technology (RMIT), Melbourne, VIC 3000, Australia. E-mail: muhammad.khalil@rmit.edu.au.
* To whom correspondence should be addressed.
Manuscript received: 2022-11-22; revised: 2022-12-22; accepted: 2022-12-26

waves produced by the RE to be sensitive to the impedance load status, which is determined by the induced current. The RE reflection coefficient measures how much power the RE reflects compared to the incident power. It is defined as the ratio of the reflected signal power to the incident signal power. In an ideal RE, the reflection coefficient should be unity, meaning there is no power loss in the RE, and all of the incident power is reflected. This is desirable because the RE is not dissipating any energy and is, therefore, more efficient. However, in practical applications, the RIS phase shifter typically has some insertion losses, meaning that the reflection coefficient is less than unity[13]. Additionally, the reflection coefficient may vary depending on the phase shift value. Therefore, recent RIS researchers considered an ideal phase-shifting model to mitigate the effects of non-ideal phase-shifting and simplify analysis. For instance, studies in Refs. [14, 15] found that the Reflection-Phase Shifter (RPS) model is an excellent Phase Shifter (PS) type for the passive RIS, as it can increase RE efficiency for narrowband and broadband applications[16]. In spite of that, using a passive RE is unlikely to provide a significant bandwidth due to the increased fading channels between the transmitter, RE, and receiver compared to a direct link between the transmitter and receiver[17].

In order to improve the limited bandwidth gains of passive RE, active REs are proposed as a potential solution[18, 19] . The active reflection element is a passive element that has been modified by adding a Reflection Amplifier (RA) and a suitable phase shifter. Active REs researches are still relatively limited, particularly on using efficient PS with RA; for example, Ref. [20] compared different aspects of active and passive IRSs without considering phase shifters' characteristics. Similarly, Refs. [19, 21, 22] utilized amplifiers to enhance the strength of the RE reflection signals, but without taking into account the PS properties. Another area for improvement in the construction of the active component is how the amplifier operates with the RE impedance loads, as most recent works used one modulation state, leading to sub-optimal operation. This is because using the amplifier in one modulation state mode leads to the amplifier switching between active and inactive states, which results in not fully utilizing the amplifier's capabilities. In order to address this issue, this paper proposes an RA that maintains active regardless of the switching load state. Such a scenario leads to optimal operation and improves various aspects of RE, including throughput, power efficiency, and coverage. An RA (negative resistance amplifier) is a device with a single input and output port known for its compact size and low profile[23]. RA devices have been proposed for use in the design of active antennas for various wireless communication scenarios[18] and have been used to improve the communication range of Radio-Frequency Identification (RFID) systems[23]. The design of RA circuits is similar to that of oscillator circuits in that both produce output without requiring input. However, RA circuits are designed to achieve an inevitable gain through negative resistance without meeting the oscillation conditions that are necessary for oscillators[23]. To fit a reflection amplifier for each RIS element, we can use it with RPS. The RPS is a type of transmission PS based on a Quadrature Hybrid Coupler (QHC), and its operation relies on two identical variable impedance loads. The QHC divides the input signal into two signals that have equal amplitudes and differ in phase by $\frac{\pi}{2}$[24], and the impedance loads then reflect each input signal. The waves reflected from the two impedance loads are combined at the output port, resulting in a change in the input signal phase.

In this paper, an active RIS design uses RA and RPS devices under two possible scenarios, denoted as Sc1 and Sc2. In the first scenario, Sc1, the RA and RPS are biased to operate simultaneously as a switch. The Sc1 strategy is similar to the active RIS design in the current literature but uses RPS as a new addition. The RPS showed a lower loss when used with the passive RE[14, 15] , increasing the efficiency of the RIS. This means that the Sc1 strategy is more effective at achieving the desired scattering properties compared to traditional active RIS designs that do not incorporate RPS. In the Sc2 Scenario, the RA remains active regardless of the switching states of RE loads, and this represents an optimal case for the active RE. The Sc1

and Sc2 scenarios are analyzed and compared in terms of various characteristics, including gain, Signal-to-Noise Ratio (SNR), insertion loss, noise figure, communication range, and power-added efficiency. The results show that Sc2 generally has higher values for these characteristics than Sc1, except for slightly higher insertion loss, but this is considered insignificant compared to the other advantages of Sc2. In order to confirm these results, numerical examples were presented to show how each scenario performed. Before continuing with the discussion, we present Table 1 that summarizes the notation used in the manuscript.

The remainder of the paper is organized as follows. Section 2 describes the system model; Section 3 demonstrates enhanced load impedance of RIS; Section 4 examines amplifying of two RPS states reflection coefficients; Section 5 shows proposed scheme characterization; Section 6 presents the simulation results; and finally, conclusion and future work are presented in Section 7.

2 System model

Consider a single transmitter (S) and a single receiver ($\mathcal{D}$) attempting to communicate with each other through a two-hop network that includes an RIS panel. The direct link between S and $\mathcal{D}$ is not feasible due to poor channel quality over a long distance. As a result, the receiver $\mathcal{D}$ can only receive the signals relayed through the RIS panel. Each of S and $\mathcal{D}$ has a single antenna with gains G_S and $G_{\mathcal{D}}$, respectively. The distance between the transmitter S and the RIS panel is referred to as r_s, and the distance between the RIS and the receiver $\mathcal{D}$ is denoted as $r_{\mathcal{D}}$. The RIS panel is located between S and $\mathcal{D}$ and consists of n reflecting elements ($n = 1, 2, \ldots, \mathcal{N}$), as illustrated in Fig. 1a. The angles of incidence and reflection of the electromagnetic waves at the RIS panel are θ_i and θ_r, respectively. The RIS panel's reflecting elements are assumed to be passive and their performance is affected by phase shifting on the incident signal. The received power at $\mathcal{D}$ is calculated using the Friis transmission formula, which gives the value

$$P_R = \left(\sqrt{|\Gamma|}\frac{\lambda}{4\pi}\right)^4 P_t \left|\sum_{n=1}^{\mathcal{N}} \sqrt{\frac{G_{S_n} G_{\mathcal{D}_n} G(\theta_{i_n}) G(\theta_{r_n})}{(r_{s_n} r_{\mathcal{D}_n})^2}}\, |\Gamma_n| \mathrm{e}^{-\mathrm{j}\left(\theta_n + \frac{2\pi}{\lambda}(r_s + r_{\mathcal{D}})\right)}\right|^2 \quad (1)$$

where P_R is the revived power by the destination node, θ_n is the adjusted phase response of the n-th elements, $G(\theta_i)$ and $G(\theta_r)$ are the antenna gains at incident and reflected signal at RIS element, respectively, and $|\Gamma|$ is the amplitude attenuation of the reflection coefficient defined by $|\Gamma| \in [0,1]$ when the RIS element is passive (see the Appendix).

By assuming that the distances r_{s_n} and $r_{\mathcal{D}_n}$ are long, then $r_{s_n} = r_s$, $r_{\mathcal{D}_n} = r_{\mathcal{D}}$, $G_{S_n} = G_S$, $G_{\mathcal{D}_n} = G_{\mathcal{D}}$, $\theta_{i_n} = \theta_i$, and $\theta_{r_n} = \theta_r$. As a result, Eq. (1) can be expressed as follows:

$$P_R = \left(\sqrt{|\Gamma|}\frac{\lambda}{4\pi}\right)^4 P_t \beta \left|\sum_{n=1}^{\mathcal{N}} |\Gamma_n| \mathrm{e}^{-\mathrm{j}(\theta_n)}\right|^2 \quad (2)$$

where $\beta = \dfrac{G_S G_{\mathcal{D}} G(\theta_i) G(\theta_r)}{(r_s r_{\mathcal{D}})^2}$.

When all REs are in phase and have the same

Table 1 Summary of notations.

Notation	Description
$G_S, G_{\mathcal{D}_n}, G(\theta_{i_n})$, and $G(\theta_{r_n})$	The gains of the antennas for the source, destination, RIS incident, and reflected signals, respectively
θ_i and θ_r	The incidence and reflected electromagnetic wave angles at each RIS element, respectively
θ_n	The adjust phase response of the n-th elements, arrived at destination node
r_s and r_D	The distances between the source and the RIS, and between the RIS and the receiver, respectively
Γ	RIS reflection coefficient
N_F	Noise factor
$\mathcal{G}$ and $\mathcal{G}^s$	Power amplifier and phase shifter gains, respectively
N_i and N_o	The input and the output noise powers
P_ϱ	Power-added efficiency
P_t and P_R	Transmitted and received powers, respectively

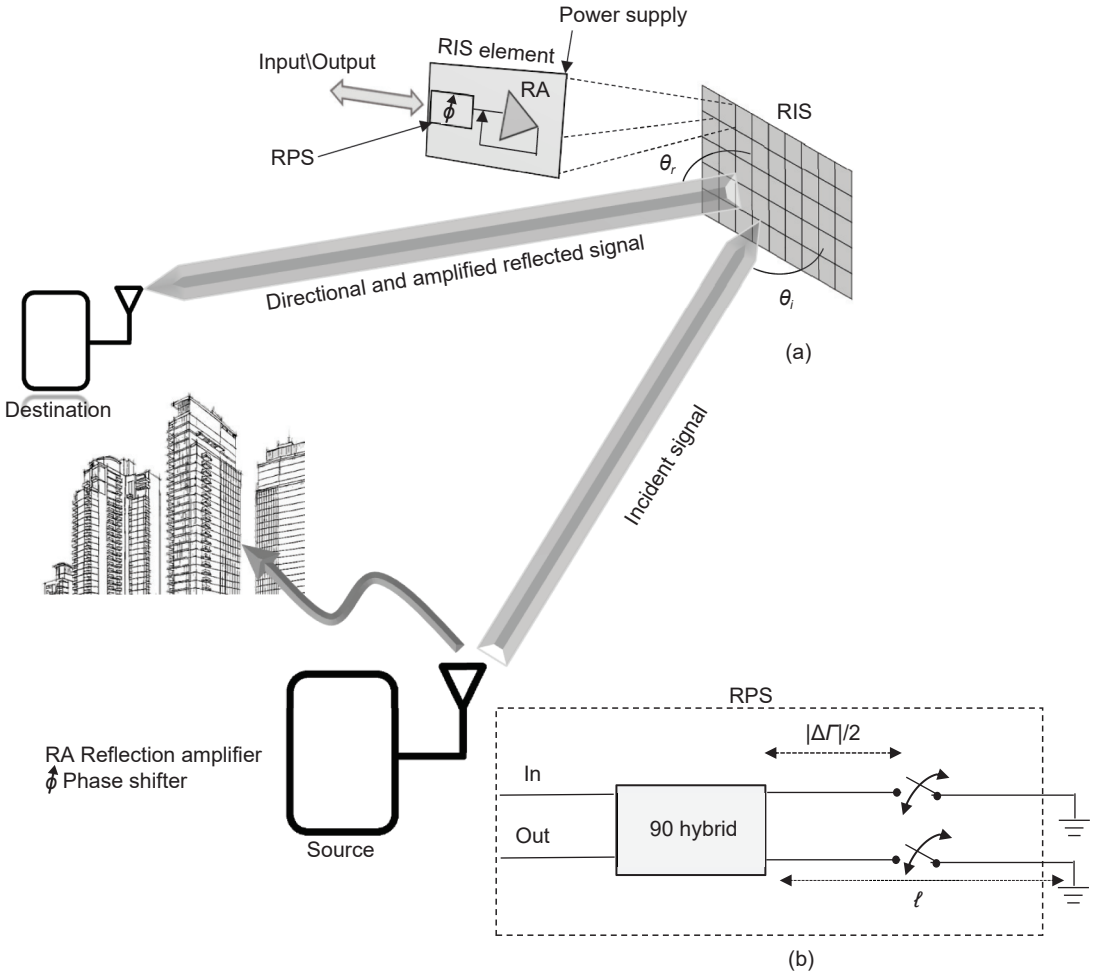

Fig. 1 System model.

reflections coefficient, i.e, $\theta_n = \theta$ and $\Gamma_n = \Gamma$, Eq. (2) can be approximated to

$$P_R = \left(\frac{\lambda}{4\pi}\right)^4 P_t \beta |\Gamma|^2 \mathcal{N}^2 \tag{3}$$

In order to calculate the received SNR, Eq. (1) is used along with the Noise Figure (N_F) metric, which measures the degradation of SNR caused by components in a signal chain. This can be expressed mathematically as $P_R = KT\mathcal{B}N_F$ (SNR), where K is Boltzmann's constant $= 1.38 \times 10^{-23}$ J/K, T is a device temperature, and $\mathcal{B}$ is the bandwidth. Then, we have

$$\text{SNR} = \frac{P_t}{KT\mathcal{B}N_F}\left(\frac{\lambda}{4\pi}\right)^4 \beta |\Gamma|^2 \mathcal{N}^2 \tag{4}$$

Equation (4) indicates that the SNR of the received signal from passive RIS elements is proportional to the $|\Gamma|$ coefficient ($|\Gamma| : 0 < |\Gamma| \leqslant 1$). The variable N_F in Eq. (4) is expressed as $N_F = 10\log(1 + \frac{N_o}{\mathcal{G}N_i})$ dB, where $\mathcal{G}$ is the amplifier gain, N_o is the output noise power, and N_i is the input noise power defined as N_i = Boltzmann's constant × noise temperature × noise bandwidth. When the amplifier is noiseless, the noise factor $(1 + \frac{N_o}{\mathcal{G}Ni})$ equals 1, i.e., N_F = 0 dB; however, in a practical environment, the amplifier and phase shifter give $N_F > 0$ dB. The phase shifter, which is assumed to be RPS in this work, affects the $|\Gamma|$ coefficient. The reflective phase shifter (i.e., RPS) consists of two ports that act as input and output, as shown in Fig. 1b. It consists of a Quadrature Hybrid (QH) and a pair of matched loads with series switches (diodes). The QH divides the incoming signal into two signals with a 90° phase difference. The switches can be turned on or off to bias the diode. When the switches are turned "on" or "off", the total path length for both reflected waves changes by an amount $\Delta\theta$, where the θ here

corresponds to θ_t. At the output port, the waves reflected from the two loads will combine in phase. Ideally, when the switches are turned on, the input signal will pass through the transmission lines ℓ (shown in Fig. 1b) and bounce back off the switches. The reflection coefficient is determined by the distance the signal traveled through ℓ[24].

3 Load impedance of RIS

The RIS panel consists of many small antennae called Reflection Elements (REs). Each RE includes diodes (either PIN or varactor) that can be biased with a tunable voltage. When the diodes are in the forward mode (turned on or short-circuited), each RE presents a small impedance to the incident signal, allowing the current to flow through it and inducing a voltage. On the other hand, when the diodes are in reverse mode (turned off), the incident current encounters a high impedance, resulting in a different reflection coefficient than a low impedance state[25]. The lowest load impedance is calculated as

$$\Gamma_H = \frac{Z_a - Z_{\text{ant}}^*}{Z_a - Z_{\text{ant}}} \tag{5}$$

where (*) represents a complex conjugate.

On the other hand, the reflection coefficient from high load impedance is given by

$$\Gamma_L = \frac{Z_b - Z_{\text{ant}}^*}{Z_b - Z_{\text{ant}}} \tag{6}$$

where Z_{ant} is the input impedance of the antenna, and Z_a and Z_b are the low and high RE impedance loads, respectively.

For the passive RE, the magnitude and the phase of both Γ_H and Γ_L are, respectively, defined as

$$\Gamma_H = |\Gamma_H| \angle\theta_H = \mathrm{e}^{\mathrm{j}\theta + \mathrm{j}\pi}, \quad |\Gamma_H| \leqslant 1 \tag{7}$$

$$\Gamma_L = |\Gamma_L| \angle\theta_L = \mathrm{e}^{\mathrm{j}\theta}, \quad |\Gamma_L| \leqslant 1 \tag{8}$$

where $|\Gamma_H|$ and $|\Gamma_L|$ are the magnitude, $\angle\theta_H$ and $\angle\theta_L$ are the reflected phase shift signals for Γ_H and Γ_L, respectively.

The maximum $|\Gamma_H|$ or $|\Gamma_L|$ in Eqs. (7) and (8) equals one when the phase difference is equal to π. Now, when the reflection coefficient is switched from Γ_H to Γ_L, the difference between them is defined as $|\Delta\Gamma| = |\Gamma_H| \angle\theta_H - |\Gamma_L| \angle\theta_L$. By applying Euler's identity on Eq. (7), it can be rewritten as

$$\Gamma_H = -\mathrm{e}^{\mathrm{j}\theta} = -\Gamma_L \tag{9}$$

Then, the difference between amplitudes of Γ_H and Γ_L is given by $|\Delta\Gamma| = |\Gamma_H - \Gamma_L|$. Since the Γ_H or Γ_L changes between "on" and "off" states (i.e., one and zero values), the maximum reflection power gives $|\Delta\Gamma| = 1$[26]. So, it has been determined that the reflection elements are affected by the load impedance. Therefore, the performance of the RIS panel can be improved by controlling the RE load impedance, which can be done using an amplifier, as shown in Fig. 2. The next step is to examine the influence of the RE load when it is connected directly to the RPS. When the RA is biased in sync with the RPS, the RE load impedance alternates between passive and active modes, as shown in Fig. 2a. In the passive state, the system reflection coefficient is observed to be

$$\Gamma_L = |\Gamma_L| \angle\theta_L = \mathfrak{B}\mathrm{e}^{\mathrm{j}\theta_L} \tag{10}$$

where $\mathfrak{B}$ is the amplitude reflection coefficient that corresponds to $|\Gamma_L|$; and if the RE works ideally, $\mathfrak{B} = 1$, otherwise, $\mathfrak{B} < 1$.

In the case of the active status, the reflection coefficient signal is amplified with a power gain as

$$\Gamma_H = |\Gamma_H| \angle\theta_H = \mathcal{G}^{0.5}\mathrm{e}^{\mathrm{j}\theta_H} \tag{11}$$

where $\mathcal{G}$ is amplifier power gain.

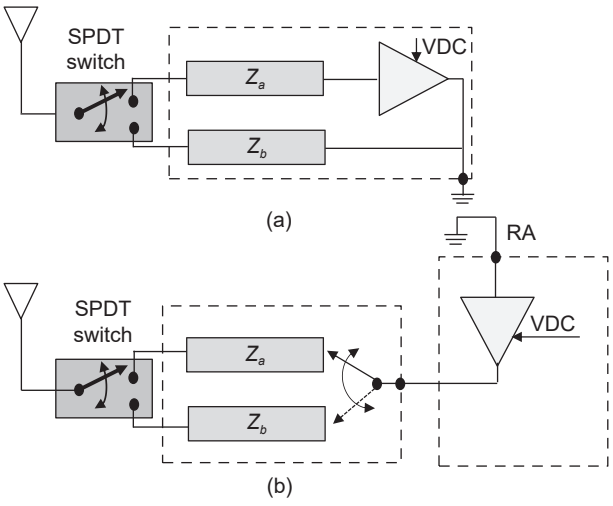

Fig. 2 (a) Active Sc1 scheme and (b) active Sc2 design.

From Eqs. (10) and (11), the value of $\Delta\Gamma$ is given by

$$\Delta\Gamma = \mathcal{G}^{0.5}\mathrm{e}^{\mathrm{j}\theta_H} - \mathfrak{B}\mathrm{e}^{\mathrm{j}\theta_L} \tag{12}$$

When $\theta_H = \theta_L$ and $\mathfrak{B} = 1$, the lowest amplitude value of Eq. (12) is given by $|\Delta\Gamma| = \mathcal{G}^{0.5} - 1$. In contrast, the maximum $\Delta\Gamma$ value can be realized at the opposite angles' site as $\theta_H = \theta_L + \pi$. Thus, Eq. (12) is given by $\Delta\Gamma = \mathcal{G}^{0.5}\mathrm{e}^{\mathrm{j}(\theta_L+\pi)} - \mathfrak{B}\mathrm{e}^{\mathrm{j}\theta_L}$, and by considering Euler's identity, we get the angles that give the maximum amplitude reflection coefficient as follows:

$$|\Delta\Gamma| = \mathcal{G}^{0.5} + 1 \tag{13}$$

According to Eq. (13), the RA is only active in one state, while the second is passive. This type of RE operation is referred to as Sc1. However, due to the RA being active in only one state, Sc1 represents a sub-optimal case.

4 Optimal RA operation

This section presents a method for optimizing the RE by fully utilizing the capabilities of the RA. To do this, the RA must be kept active constantly, regardless of the switching load state, as shown in Fig. 2b. In order to identify the conditions that allow the RA to continue operating, the scattering parameters (*S*-parameters) are analyzed. The gain of the amplifier can then be calculated as follows:

$$\Gamma = S_{11}^{a} = \frac{\text{Reflected signal power}}{\text{Incident signal power}} \tag{14}$$

where S_{11}^{a} is the signal reflection coefficient and equivalent to $S_{11}^{a} = \left|S_{11}^{a}\right|\angle\theta_{11}$, and $\angle\theta_{11}$ is the phase value $\angle\theta_{11} \in \{\theta_L, \theta_H\}$.

When an amplifier is not in negative resistance mode, the scattering parameter S_{11}^{a} represents a loss. However, when the amplifier is operating in negative resistance mode (also known as a reflection amplifier), S_{11}^{a} represents a positive gain.

Since the RA is interconnected to a phase shifter, it is necessary to determine the transmission parameter $\left(S_{21}^{s}\right)$ of the phase shifter using the following definition:

$$T^{s} = S_{21}^{s} = \frac{\text{Transmission signal power}}{\text{Incident signal power}} = \left|S_{21}^{s}\right|\angle\theta_{21},\ 0 < S_{21}^{s} < 1 \tag{15}$$

where $\angle\theta_{21}$ is the phase shift signal $\angle\theta_{21} \in \{\theta_L, \theta_H\}$.

In an ideal scenario, a phase shifter should maintain the same signal strength $\left|S_{21}^{s}\right|$ while changing the phase (θ). However, in practice, phase shifters may experience losses over a wide range of phase shifts. These losses can be characterized by the insertion loss, which is typically expressed in decibels[13] represented as $-10\log\left(1/\left|S_{21}^{s}\right|^2\right)$, or by its gain $\mathcal{G}^{s}$, which is a ratio or coefficient indicating as $\mathcal{G}^{s} = 10\log\left|S_{21}^{s}\right|^2$. These losses may depend on the design and operating conditions of the phase shifter.

By combining RA directly to RPS, the total gain is produced as[27]

$$\left[S_{11}^{\mathcal{T}}\right] = \left[S_{21}^{s}\right]\left[S_{11}^{a}\right]\left[S_{21}^{s}\right] \tag{16}$$

As mentioned earlier, an input signal to the RPS divides equally between the two ports, with the phase 0^{o} and $\frac{\pi}{2}$. Thus, the S_{21}^{s} at each port is

$$\left[S_{21}^{s}\right] = \begin{bmatrix} \left|S_{21}^{s}\right|\mathrm{e}^{\mathrm{j}0} & \left|S_{21}^{s}\right|\mathrm{e}^{\mathrm{j}\frac{\pi}{2}} \end{bmatrix} \tag{17}$$

where $\left|S_{21}^{s}\right| = 1$.

When the RA keeps active during any RPS statuses, the S_{11}^{a} is then defined by

$$\left[S_{11}^{a}\right] \triangleq \begin{bmatrix} \mathcal{G}^{0.5}\mathrm{e}^{\mathrm{j}\theta_H} & \mathcal{G}^{0.5}\mathrm{e}^{\mathrm{j}\theta_L} \end{bmatrix} \tag{18}$$

where $\mathcal{G}^{0.5}\mathrm{e}^{\mathrm{j}\theta_L}$ can be be obtained, as $-\mathcal{G}^{0.5}\mathrm{e}^{\mathrm{j}\theta_H}$, in the same form in which Eq. (9) obtained.

By using the identity matrix for Eqs. (17) and (18) and considering Euler's identity, the value $\left[S_{11}^{\mathcal{T}}\right]$ is obtained as follows:

$$\begin{aligned} \left[S_{11}^{\mathcal{T}}\right] &= \begin{bmatrix} \mathrm{e}^{\mathrm{j}\frac{\pi}{2}} & 0 \\ 0 & 1 \end{bmatrix}^{-1} \begin{bmatrix} \mathcal{G}^{0.5}\mathrm{e}^{\mathrm{j}\theta_H} & 0 \\ 0 & -\mathcal{G}^{0.5}\mathrm{e}^{\mathrm{j}\theta_H} \end{bmatrix} \\ \begin{bmatrix} \mathrm{e}^{\mathrm{j}\frac{\pi}{2}} & 0 \\ 0 & 1 \end{bmatrix} &= \begin{bmatrix} \mathcal{G}^{0.5}\mathrm{e}^{\mathrm{j}\theta_H} & 0 \\ 0 & -\mathcal{G}^{0.5}\mathrm{e}^{\mathrm{j}\theta_H} \end{bmatrix} \end{aligned} \tag{19}$$

where $[\cdot]^{-1}$ is the matrix inverse.

Equation (19) reveals that both $\Gamma_L = -\mathcal{G}^{0.5}\mathrm{e}^{\mathrm{j}\theta_H}$ and $\Gamma_H = \mathcal{G}^{0.5}\mathrm{e}^{\mathrm{j}\theta_H}$ are more significant than one depending on $\mathcal{G}$; thereby

$$|\Delta\Gamma| = \left|-\mathcal{G}^{0.5} - \mathcal{G}^{0.5}\right| = (4\mathcal{G})^{0.5} \tag{20}$$

The design described in Eq. (20) is referred to as Sc2 and is considered optimal for RIS operation because it enables continuous amplification of the reflected signals.

5 Proposed scheme characterization

In order to compare the features of Sc1 and Sc2, this section presents a comparison of Sc2 and Sc1 based on various characteristics relevant to RIS operation, including insertion loss, signal-to-noise ratio, distance, and amplifier efficiency.

The total insertion loss power for the transfer signal between RPS and the reflected amplifier is given as

$$\left|\Delta\Gamma\right|_{\text{loss}}\Big|_{\text{Sc2}} = (T^s)^{0.5}\,|\Delta\Gamma|\,(T^s)^{0.5} = T^s\,(4\mathcal{G})^{0.5} \tag{21}$$

Now, if we calculate insertion loss power for Sc1 $\left(\left|\Delta\Gamma\right|_{\text{loss}}\Big|_{\text{Sc1}}\right)$, we can obtain it as $\left|\Delta\Gamma\right|_{\text{loss}}\Big|_{\text{RPS-S1}} = T^s\left(\mathcal{G}^{0.5}+1\right)$. It is clear that the insertion loss for Eq. (21) is slightly higher than that of Sc1 i.e., $T^s\,(4\mathcal{G})^{0.5} > T^s\left(\mathcal{G}^{0.5}+1\right)$. By comparing the insertion loss of Sc1 and Sc2, we get

$$\left|\Delta\Gamma\right|_{\text{loss}}\Big|_{\text{Sc2}} \Big/ \left|\Delta\Gamma\right|_{\text{loss}}\Big|_{\text{Sc1}} = \sqrt{4\mathcal{G}}\Big/\left(\mathcal{G}^{0.5}+1\right) \tag{22}$$

Increasing $\mathcal{G}$ in Eq. (22) leads to higher insertion losses in Sc2 compared to Sc1. As a result, the insertion loss of Sc2 is a disadvantage compared to Sc1 and should be kept as low as possible. By substituting the value of $|\Delta\Gamma|$ determined by Eqs. (13) and (20) into Eq. (4), we can compare the SNR of Sc1 and Sc2. Since SNR is proportional to $|\Delta\Gamma|$[28], the following mathematical expression can be then derived as

$$\text{SNR}_{\text{Sc2}}/\text{SNR}_{\text{Sc1}} = 4\mathcal{G}\Big/\left(\mathcal{G}^{0.5}+1\right)^2 \tag{23}$$

where SNR_{Sc1} and SNR_{Sc2} are the SNR of Sc1 and Sc2 scenarios, respectively.

In Fig. 3a, the term of $\text{SNR}_{\text{Sc2}}/\text{SNR}_{\text{Sc1}}$ is plotted and

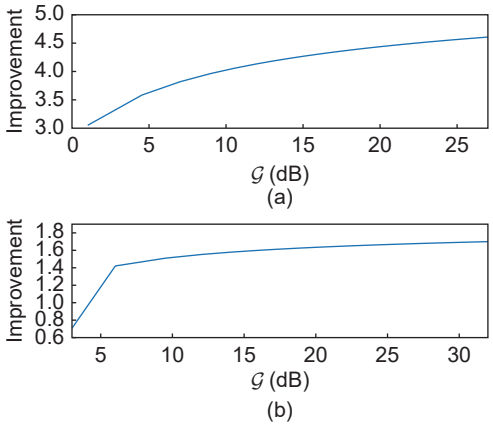

Fig. 3 Improvement of (a) $\text{SNR}_{\text{Sc2}}/\text{SNR}_{\text{Sc1}}$, and (b) $d_{\text{bSc2}}/d_{\text{aSc1}}$.

it is demonstrated that there is a logarithmic relationship with $\mathcal{G}$ but at low $\mathcal{G}$ values, the relationship becomes linear. As a result, Sc2 leads to a higher SNR than Sc1, and the SNR is higher at low values of $\mathcal{G}$.

Given a higher SNR in Eq. (23), the reflection coefficient provided by Sc2 is stronger than Sc1. As a result, the propagation range of Sc2 is also greater. To express the relationship between the range of Sc1 and Sc2 mathematically, we can use the total distance of Eq. (3) as follows:

$$r_s r_{\mathcal{D}} = \left(\frac{\lambda}{4\pi}\right)^2 \mathcal{N}\,|\Gamma|\,\sqrt{P_t G_S G_{\mathcal{D}} G(\theta_i) G(\theta_r)/P_R} \tag{24}$$

Let the distance d_a $(d_a \in (r_s, r_{\mathcal{D}}))$ represent the total allowable distance for the scenario Sc1 in Eq. (20) and d_b $(d_b \in (r_s, r_{\mathcal{D}}))$ for the Sc2 scenario under Eq. (13) design. Then, the improvement range between Sc1 and Sc2 for each RE is given by

$$d_{\text{bSc2}}/d_{\text{aSc1}} = \sqrt{4\mathcal{G}/\left(\mathcal{G}^{0.5}+1\right)^2} \tag{25}$$

where d_{aSc1} and d_{bSc2} are the d_a and d_b of Sc1 and Sc2 scenarios, respectively.

The plot of Eq. (25) in Fig. 3b shows that the low amplifier gain results in a long distance for d_{bSc2} compared to d_{aSc1}. However, there is a significant increase at $\mathcal{G} > 8$, which indicates that Sc2 provides better coverage than Sc1, particularly at low power gain.

Since the proposed RIS panel uses a VDC power supply to provide DC energy for all components, with the majority of energy consumed by the amplifier (RA), it is essential to calculate the amplifier's efficiency (η) to optimize energy usage[29]. The η is defined as the ratio of the output power P_R to the power provided by the DC supplier, and it can be expressed as $\eta = \dfrac{1}{1+\dfrac{1}{P_R}(P_\sigma - P_t)}$, where P_σ is the power that is dissipated and not converted to P_R, which is defined as $P_\sigma = (P_t + P_{\text{dc}}) - P_R$. When we need to determine how much the DC input power contributes to the amplification of an input signal, the amplifier efficiency is then called power-added efficiency (P_ϱ), and it is formulated as $P_\varrho = \left(1-\dfrac{1}{\Gamma}\right)\eta$. Now, let $P_{\varrho\text{Sc1}}$ be

the power-added efficiency when the RIS works according to the Sc1 model, and it is $P_{\varrho Sc2}$ for Sc2. By comparing $P_{\varrho Sc1}$ to $P_{\varrho Sc2}$, we can obtain

$$P_{\varrho Sc2}/P_{\varrho Sc1} = \left(2\mathcal{G} + \mathcal{G}^{0.5} - 1\right)/2\mathcal{G} \tag{26}$$

Equation (26) indicates that the $P_{\varrho Sc2}$ is higher than $P_{\varrho Sc1}$ at any gain level, which means Sc2 is lower energy consumption than Sc1. To confirm such a result, we can use Eqs. (4) and (23) to plot the relationship between RE energy consumption and SNR, as shown in Fig. 4. Figure 4 assumes that the distance is 900 m and $\mathcal{G} = 8$ dB. It is seen that the lowest energy consumption appeared at the operating SNR range −3 dB to 3 dB for all link distances; this is because transmission power is in a realistic, moderate scale. For SNR levels lower than −3 dB, the energy consumption rises due to high noise. In contrast, for SNR levels higher than 3 dB, the transmit power must be high, leading to increased energy consumption. However, for any levels above 3 dB or low −3 dB, the Sc2 energy consumption is lower than Sc1, indicating a stronger signal and less noise. Generally, a device or system with a higher P_{ϱ} will have lower energy consumption than one with a lower P_{ϱ} if both devices perform the same task. This is because a higher P_{ϱ} indicates that the device is more efficient in converting input power into output power, which means that it will require less input power to perform the same task. It is worth mentioning here that P_{ϱ} is a measure of efficiency and does not consider the total amount of work being performed. Therefore, a device with a higher P_{ϱ} may still consume more energy than a device with a lower P_{ϱ} if it is performing more work or operating for a longer period.

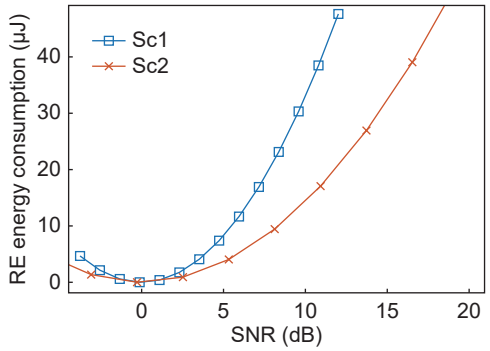

Fig. 4 Relationship between energy consumption and SNR for Sc1 and Sc2.

6 Numerical results and discussions

This section implements numerical simulations to evaluate the proposed Sc1 and Sc2 models. The analytical results are verified using Matlab and Advanced Design System (ADS) simulation tools. The block diagram for simulation mode is illustrated in Fig. 5, which includes three stages SPDT switch, RPS, and RA. The last stage consists of an RA circuit which is designed and implemented experimentally by many studies such as Refs. [30, 31]. Thus we employed RA designed of Ref. [31] in our simulation by using ADS. An RA circuit is a single port device consisting of a negative resistance terminating, amplifying, and reflecting a wave incident upon it. Designing RA circuits is similar to oscillator device patterns, as the desired RA gain (i.e., $\mathcal{G}$) is produced by creating a negative resistance in the absence of the requirements for oscillating conditions. This attribute allows the RA to operate at low input power[32, 33].

By applying several incident power levels and bias voltages, the output reflection coefficient of RA is measured according to Eqs. (13) and (20) as shown in Fig. 6. The biasing voltage (V_i) was tuned between two VDC configurations: V_1=1.02 V and V_2=1.004 V. The used operation frequency is 2.34 GHz; and the

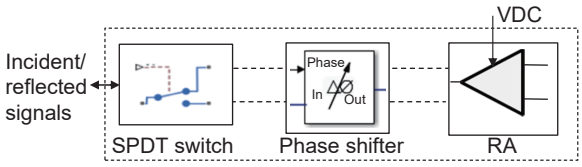

Fig. 5 Simulation block diagram of each RE.

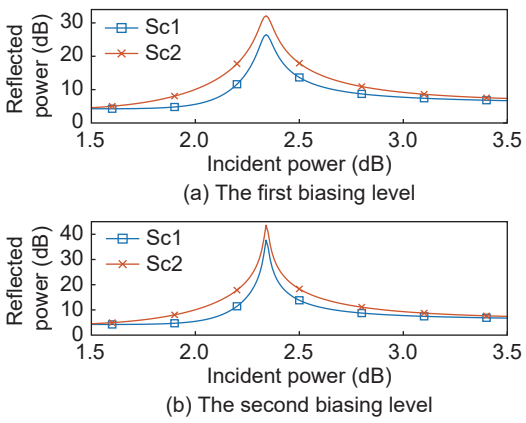

Fig. 6 Reflection gain.

reflection coefficient gains were controlled by the VDC biasing. It is worth mentioning that any spectrum bands can be adopted rather than the frequency range employed for this work. The Sc1 and Sc2 reflection gains were obtained directly by using the *S*-parameters function in Matlab and setting the RIS incident power to −35 dB.

The RA is designed to exhibit negative resistance after the transistor reaches the breakdown voltage, and then the relationship between voltage and output current becomes inverse[34]. As a result, the RA gain is increased by reducing biasing voltage, and this is proven in Fig. 6b. In Fig. 6b, the reflection gains are obtained at different incident power levels. It is clearly shown that the Sc2 reflection power gain is higher than that of Sc1. The Sc2 gain is further raised by downward biasing from V_1 to V_2. The Sc2 results in Fig. 6 confirm the proposed analytical in Eq. (20), which reveals that Sc2 gain is higher than Sc1 in Eq. (13). By comparing the above results with what is observed by Refs. [18, 35], we can see that the gain of Sc1 and Sc2 shows the range between 38 and 43 dB under 1.004 V biasing, while Ref. [18] used a bias voltage of 7.25 V to achieve a maximum reflection of 30 dB. Furthermore, Refs. [18, 35] are limited to active RIS elements by using Sc1, while our proposed method gives more flexibility by using biasing voltages to provide different power gains. In this case, the linear amplifier regions and the saturation regions vary with the operation mode of the power amplifier.

Typically, it is preferred for the RA to operate at the maximum linear region because its operation in the nonlinear area leads to generating a distortion and harmonics in the output wave[36]. To compare the linearity of Sc1 and Sc2, Fig. 7 depicts the adequate output power (reflected power gain), which is measured by calculating the difference between the output power delivered by the amplifier and the incident power that the amplifier can handle. It is clearly shown that the length of the reflected power of Sc2 (black arrow) is higher than that of Sc1 for any biasing level. Higher gain with Sc2 design leads to lower N_F at each V_i level, as increasing gain reduces noise, as shown in Fig. 8. We can also see that the

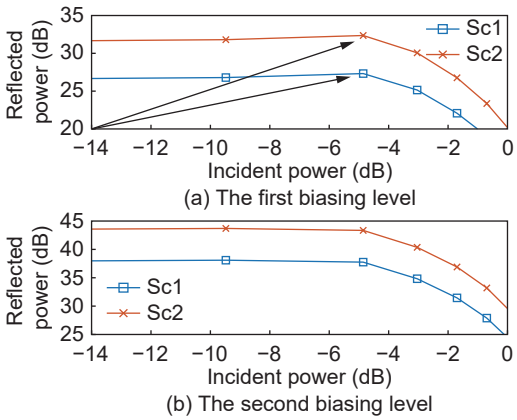

Fig. 7 Gain compression point (black arrow represents the reflected power).

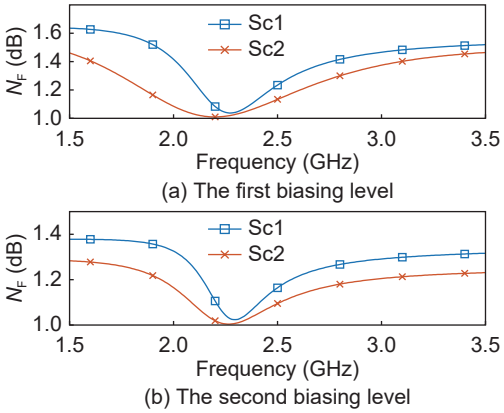

Fig. 8 Noise figure for two biasing levels.

minimum N_F point is allocated at the range of 2.3 GHz, and at this point, the shot and thermal noise is raised to a higher level[37]. Increasing RA reflection gain also provides high reflected power for each RIS element, as shown in Fig. 9, which illustrates the relationship between reflected SNR and incident power. It indicates

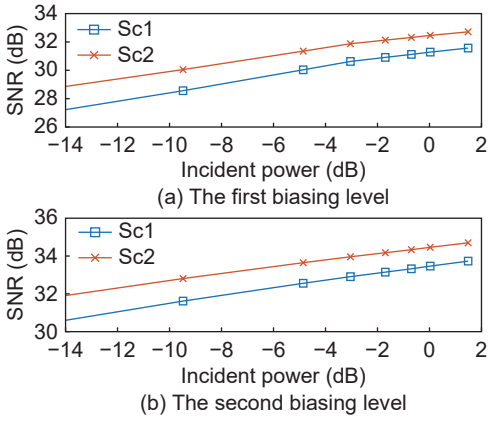

Fig. 9 SNR vs. incident power.

that the SNR of Sc2 is higher than that of Sc1, and this is the expected result because Sc2 reflected gain is more elevated than Sc1. The output power equals reflected gain plus incident power.

The high SNR increases the achievable rate provided by each RIS element, and this is illustrated in Fig. 10. Figure 10 also shows that in the low incident power range (i.e., the range between −35 and −25 dB), Sc2 delivers 0.43 bps/Hz higher than Sc1, while the incident power range is between −20 and 0 dB, and the different rate becomes 0.27 bps/Hz. This result confirms our theoretical analysis in Eq. (23), which shows that the Sc2 scheme is higher than Sc1 in the linear region. Such a range represents the low-input power range. Reference [38] reported that increasing incident power decreases gain due to the negative resistance, the behavior of which is greatly affected by its bias point. Thus, Sc2 is preferable to Sc1 in low-input power operations. A similar result is evident in the V_2 scenario. As Fig. 10b demonstrates, the incident power range of −35 to −25 dB gives a different rate of 0.33 bps/Hz, while the range between −20 to 0 dB is 0.23 bps/Hz. Accordingly, the data rate gaps between Sc1 and Sc2 are reduced by increasing system gain. The example in Fig. 10 considered the distance from the source to destination as 1 m, and the achievable rate of each RIS element is 40 to 50 bps/Hz. By increasing the distance to 800 m, the data rate reduces to 3.0 and 3.2 bps/Hz, as shown in Fig. 11. In each biasing case, the achievable rate in Sc2 is higher than Sc1 by the range of 0.33 to 0.43 bps/Hz. Thus, if we use 200 RIS elements, we expect to get 66 to 86 bps/Hz, and this result agrees with what was presented in Ref. [18].

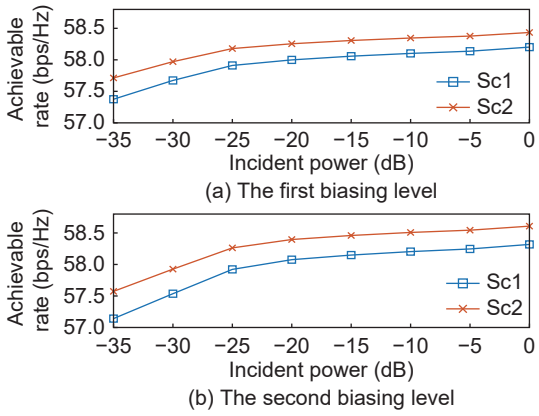

Fig. 10 Achievable rate.

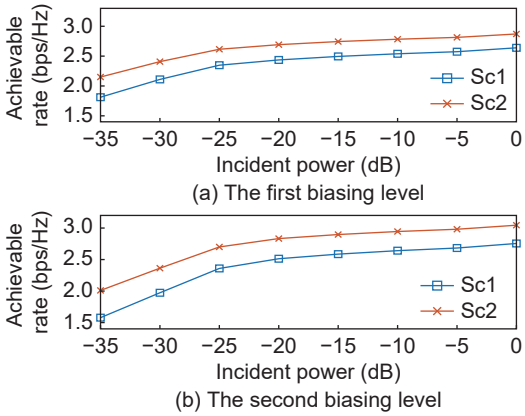

Fig. 11 Achievable rate by each element RE.

To determine how much the VDC input power contributes to the amplification of an incident signal, Fig. 12 shows the P_{ϱ} in terms of the incident signal. In the case of a constant amplitude signal, the amplifier is continuously operating at its peak efficiency point. When the signal has a high peak-to-average ratio and, thus, a varying envelope, the amplifier is forced to operate in less efficient regions, as shown in Fig. 12b. When a constant amplitude signal is amplified, the amplifier always operates at its peak efficiency point. If an amplifier has high efficiency, all its incident power is converted into output power. Figure 12 clearly shows that the P_{ϱ} of Sc2 is always higher than that of Sc1. Then the RE energy consumption in Sc2 is lower than Sc1 scenario.

7 Conclusion

This paper presents a study on improving the performance of RE by incorporating RA and RPS into

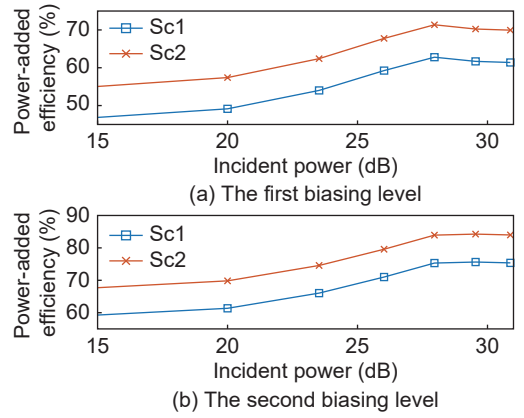

Fig. 12 P_{ϱ} vs. incident power.

each RIS element design. The proposed scheme is demonstrated through two implementations of an active RIS element, which are Sc1 and Sc2. These scenarios impose different constraints on the reflection coefficient of the RIS elements. In Sc1, the RA operates simultaneously with RE load impedance as a switch, while in Sc2, the RA remains active regardless of the RE load impedance. The Sc1 and Sc2 designs are analysed and compared based on various characteristics such as gain, signal-to-noise ratio, insertion loss, noise figure, communication range, and power-added efficiency. The results show that Sc1 provides an active mode but is in suboptimal condition because RA was not fully utilised. On the other hand, the full capabilities of the RA are used by the Sc2 and thus provide higher features than Sc1, particularly in low incident power. Overall, the study's results suggest that the Sc2 design is the most suitable for applications requiring high performance in low incident power.

Appendix

The electric field at the RIS panel is given by Ref. [28] as follows:

$$E_n = f_n \mathrm{e}^{-\mathrm{j}\left(\frac{2\pi}{\lambda}\right) r_s} a_o \tag{A1}$$

where λ is the wavelength, a_o is the unitary vector orthogonal to the RIS plane, and f_n is the incident electric field amplitudes defined by

$$f_n = \frac{(\dot{\eta} P_t G_t)^{\frac{1}{2}}}{\sqrt{2\pi} r_s} \tag{A2}$$

where P_t is the transmitter power and $\dot{\eta}$ is the impedance of free-space.

Now, the signal intensity at any RIS element is given by $I_n = \left(\frac{f_n}{\sqrt{2\dot{\eta}}}\right)^2$. So, substituting Eq. (A2) into I_n gives

$$I_n = \frac{P_t G_S}{4\pi r_s^2} \tag{A3}$$

The intensity of radiant energy is the power transferred per unit, and this can be expressed as $I_n A_n = f_n$, where A_n is the effective aperture of the n-th RIS element. For the incident RE, it can be expressed as $A_n = \frac{\lambda^2}{4\pi} G(\theta_i)$. Then, the incident power intensity at any RE is calculated as

$$I_n = \left(\frac{\lambda}{4\pi} \frac{\sqrt{P_t G_{S_n} G(\theta_{i_n})}}{r_s}\right)^2 \tag{A4}$$

The RE reflected signal intensity (I_r) is given by $I_n \frac{\Gamma^2 G(\theta_r)}{4\pi r_{\mathcal{D}}^2}$. So considering Eq. (A4) gives

$$I_r = \left(\frac{\lambda}{4\pi r_s r_{\mathcal{D}}}\right)^2 \frac{P_t \Gamma^2 G_{S_n} G(\theta_{i_n}) G(\theta_{r_n})}{4\pi} \tag{A5}$$

The value of Γ is considered to be the same of all RIS elements. At the $\mathcal{D}$-node, the received power intensity from the n -th RIS elements is given by $I_R = I_r \frac{\lambda^2}{4\pi} G_{\mathcal{D}}$. Then, using Eq. (A5) gives

$$I_R = \left(\sqrt{\frac{\Gamma}{r_s r_{\mathcal{D}}}} \frac{\lambda}{4\pi}\right)^4 P_t \Gamma^2 G_{S_n} G_{\mathcal{D}_n} G(\theta_{i_n}) G(\theta_{r_n}) \tag{A6}$$

Furthermore, the total electric field of reflected signals is corresponding to

$$\mathcal{E} = \sum_{n=1}^{\mathcal{N}} A_{\mathrm{n}\mathcal{D}} \mathrm{e}^{-\mathrm{j}\left(\theta_n + \frac{2\pi}{\lambda}(r_s + r_{\mathcal{D}})\right)_{b_o}} \tag{A7}$$

where $\mathcal{E}$ is the bit energy, b_o is the unitary vector, and $A_{\mathrm{n}\mathcal{D}}$ is the electric field amplitude of reflected signal given by $A_{\mathrm{n}\mathcal{D}} = (2\dot{\eta} I_R)^{\frac{1}{2}}$. Substituting Eq. (A6) into $A_{\mathrm{n}\mathcal{D}}$ and then into Eq. (A7) gives

$$\mathcal{E} = \left(\sqrt{2P_t\dot{\eta}}\right)\left(\frac{\lambda}{4\pi}\right)^2 \sum_{n=1}^{\mathcal{N}} \sqrt{\frac{2\eta P_t G_{S_n} G_{\mathcal{D}_n} G(\theta_{i_n}) G(\theta_{r_n})}{(r_{s_n} r_{\mathcal{D}_n})^2}} \Gamma_n \mathrm{e}^{-\mathrm{j}(\theta_n)} \mathrm{e}^{-\frac{2\pi}{\lambda}(r_s + r_{\mathcal{D}})} \tag{A8}$$

Then the received power by $\mathcal{D}$-node is obtained by using $P_R = |\mathcal{E}|^2 / 2\dot{\eta}$, and Eq. (1) is obtained.

References

[1] M. A. ElMossallamy, H. Zhang, L. Song, K. G. Seddik, Z. Han, and G. Y. Li, Reconfigurable intelligent surfaces for wireless communications: Principles, challenges, and opportunities, *IEEE Transactions on Cognitive Communications and Networking*, vol. 6, no. 3, pp. 990–1002, 2020.

[2] S. Venkatesh, X. Lu, H. Saeidi, and K. Sengupta, A high-speed programmable and scalable terahertz holographic metasurface based on tiled CMOS chips, *Nature Electronics*, vol. 3, pp. 785–793, 2020.

[3] S. Xu, J. Liu, and J. Zhang, Resisting undesired signal through IRS-based backscatter communication system, *IEEE Communications Letters*, vol. 25, no. 8, pp. 2743–2747, 2021.

[4] M. D. Renzo, A. Zappone, M. Debbah, M. -S. Alouini, C. Yuen, J. D. Rosny, and S. Tretyakov, Smart radio environments empowered by reconfigurable intelligent surfaces: How it works, state of research, and the road ahead, *IEEE Journal on Selected Areas in Communications*, vol. 38, no. 11, pp. 2450–2525, 2020.

[5] E. Basar, M. D. Renzo, J. D. Rosny, M. Debbah, M. -S. Alouini, and R. Zhang, Wireless communications through reconfigurable intelligent surfaces, *IEEE Access*, vol. 7, pp. 116753–116773, 2019.

[6] L. Dai, B. Wang, M. Wang, X. Yang, J. Tan, S. Bi, S. Xu, F. Yang, Z. Chen, M. D. Renzo, et al., Reconfigurable intelligent surface-based wireless communications: Antenna design, prototyping, and experimental results, *IEEE Access*, vol. 8, pp. 45913–45923, 2020.

[7] P. Wang, J. Fang, X. Yuan, Z. Chen, and H. Li, Intelligent reflecting surface-assisted millimeter wave communications: Joint active and passive precoding design, *IEEE Transactions on Vehicular Technology*, vol. 69, no. 12, pp. 14960–14973, 2020.

[8] S. Li, B. Duo, X. Yuan, Y. -C. Liang, and M. D. Renzo, Reconfigurable intelligent surface assisted UAV communication: Joint trajectory design and passive beamforming, *IEEE Wireless Communications Letters*, vol. 9, no. 5, pp. 716–720, 2020.

[9] C. Huang, A. Zappone, G. C. Alexandropoulos, M. Debbah, and C. Yuen, Reconfigurable intelligent surfaces for energy efficiency in wireless communication, *IEEE Transactions on Wireless Communications*, vol. 18, no. 8, pp. 4157–4170, 2019.

[10] J. Park, B. G. Jeong, S. Kim, D. Lee, J. Kim, C. Shin, C. Lee, T. Otsuka, J. Kyoung, S. Kim, et al., All-solid-state spatial light modulator with independent phase and amplitude control for three-dimensional lidar applications, *Nature Nanotechnology*, vol. 16, pp. 69–76, 2021.

[11] S. Gong, X. Lu, D. T. Hoang, D. Niyato, L. Shu, D. I. Kim, and Y. -C. Liang, Toward smart wireless communications via intelligent reflecting surfaces: A contemporary survey, *IEEE Communications Surveys & Tutorials*, vol. 22, no. 4, pp. 2283–2314, 2020.

[12] Q. Wu and R. Zhang, Towards smart and reconfigurable environment: Intelligent reflecting surface aided wireless network, *IEEE Communications Magazine*, vol. 58, no. 1, pp. 106–112, 2020.

[13] B. S. Yarman, Fundamentals of digital phase shifters, in *Design of Digital Phase Shifters for Multipurpose Communication Systems*, B. S. Yarman, ed. New York, NY, USA: River Publishers, 2019, pp. 1–18.

[14] S. Abeywickrama, R. Zhang, Q. Wu, and C. Yuen, Intelligent reflecting surface: Practical phase shift model and beamforming optimization, *IEEE Transactions on Communications*, vol. 68, no. 9, pp. 5849–5863, 2020.

[15] Y. Shang, Q. Zeng, W. Cui, X. Wang, and G. Zheng, Design of pattern reconfigurable patch antenna array based on reflective phase-shifter, *International Journal of Antennas and Propagation*, vol. 2022, p. 2803285, 2022.

[16] I. Bahl, *Control Components Using Si, GaAs, and GaN Technologies*. Boston, MA, USA: Artech House, 2014.

[17] M. Najafi, V. Jamali, R. Schober, and H. V. Poor, Physics-based modeling and scalable optimization of large intelligent reflecting surfaces, *IEEE Transactions on Communications*, vol. 69, no. 4, pp. 2673–2691, 2021.

[18] Z. Zhang, L. Dai, X. Chen, C. Liu, F. Yang, R. Schober, and H. V. Poor, Active RIS vs. passive RIS: Which will prevail in 6G? arXiv preprint arXiv: 2103.15154, 2021.

[19] R. Long, Y. -C. Liang, Y. Pei, and E. G. Larsson, Active reconfigurable intelligent surface-aided wireless communications, *IEEE Transactions on Wireless Communications*, vol. 20, no. 8, pp. 4962–4975, 2021.

[20] C. You and R. Zhang, Wireless communication aided by intelligent reflecting surface: Active or passive, *IEEE Wireless Communications Letters*, vol. 10, no. 12, pp. 2659–2663, 2021.

[21] H. Song, M. Zhang, J. Gao, and C. Zhong, Unsupervised learning-based joint active and passive beamforming design for reconfigurable intelligent surfaces aided wireless networks, *IEEE Communications Letters*, vol. 25, no. 3, pp. 892–896, 2021.

[22] H. Chen, G. Yang, and Y. -C. Liang, Joint active and passive beamforming for reconfigurable intelligent surface enhanced symbiotic radio system, *IEEE Wireless Communications Letters*, vol. 10, no. 5, pp. 1056–1060, 2021.

[23] P. Chan and V. Fusco, Full duplex reflection amplifier tag, *IET Microwaves*, *Antennas & Propagation*, vol. 7, no. 6, pp. 415–420, 2013.

[24] C. -S. Lin, S. -F. Chang, C. -C. Chang, and Y. -H. Shu, Design of a reflection-type phase shifter with wide relative phase shift and constant insertion loss, *IEEE Transactions on Microwave Theory and Techniques*, vol. 55, no. 9, pp. 1862–1868, 2007.

[25] B. S. Yarman, Loaded line digital phase shifters, in *Design of Digital Phase Shifters for Multipurpose Communication Systems*, B. S. Yarman, ed. New York, NY, USA: River Publishers, 2019, pp. 101–184.

[26] S. Shen, B. Clerckx, and R. Murch, Modeling and architecture design of reconfigurable intelligent surfaces using scattering parameter network analysis, *IEEE Transactions on Wireless Communications*, vol. 21, no. 2, pp. 1229–1243, 2022.

[27] R. E. Anderson, S-parameter techniques for faster, more accurate network design, https://www.phys.hawaii.edu/

~idlab/taskAndSchedule/5989-9273EN.pdf, 2022.

[28] F. T. Ulaby, D. G. Long, W. Blackwell, C. Elachi, A. Fung, C. Ruf, K. Sarabandi, H. Zebker, and J. V. Zyl, *Microwave Radar and Radiometric Remote Sensing*. Ann Arbor, MI, USA: University of Michigan Press, 2014.

[29] B. Banyamin, B. Virdee, and A. Virdee, *Broadband Microwave Amplifiers*. Boston, MA, USA: Artech House, 2004.

[30] F. Farzami, S. Khaledian, B. Smida, and D. Erricolo, Reconfigurable dual-band bidirectional reflection amplifier with applications in van atta array, *IEEE Transactions on Microwave Theory and Techniques*, vol. 65, no. 11, pp. 4198–4207, 2017.

[31] J. Kimionis, A. Georgiadis, A. Collado, and M. M. Tentzeris, Enhancement of RF tag backscatter efficiency with low-power reflection amplifiers, *IEEE Transactions on Microwave Theory and Techniques*, vol. 62, no. 12, pp. 3562–3571, 2014.

[32] J. W. Boyles, The oscillator as a reflection amplifier—An intuitive approach to oscillator design, *Microwave Journal*, vol. 29, no. 6, p. 83, 1986.

[33] M. M. Ahmadi and M. Salehi-Sirzar, A self-tuned class-e power oscillator, *IEEE Transactions on Power Electronics*, vol. 34, no. 5, pp. 4434–4449, 2019.

Muhammad I. Khalil received the bachelor degree in electrical engineering from University of Mosul in 2000, the master degree in electrical engineering from University of Baghdad in 2006, and the PhD degree in electrical and electronic engineering from University of Auckland, New Zealand in 2017. He is a researcher in the School of Electrical and Electronic Engineering, University of Royal Melbourne Institute of Technology (RMIT), Australia. Before joining RMIT, he was a postdoctoral researcher at University of New South Wales, Australia. His research is situated in the communication and network systems field, focusing on the next-generation mobile and wireless networks, vehicular communications systems, and intelligent and converged networks. He worked as a senior lecturer at the Department of Electrical Engineering, University of Mosul, where he taught various computer and network courses to electrical and electronic engineering students.

[34] C. M. Grens, A comprehensive study of safe-operating-area, biasing constraints, and breakdown in advanced SiGe HBTs, https://smartech.gatech.edu/handle/1853/7124, 2005.

[35] M. H. Khoshafa, T. M. N. Ngatched, M. H. Ahmed, and A. R. Ndjiongue, Active reconfigurable intelligent surfaces-aided wireless communication system, *IEEE Communications Letters*, vol. 25, no. 11, pp. 3699–3703, 2021.

[36] G. Z. E. Nashef, F. Torres, S. Mons, T. Reveyrand, T. Monediere, E. Ngoya, and R. Quere, EM/circuit mixed simulation technique for an active antenna, *IEEE Antennas and Wireless Propagation Letters*, vol. 10, pp. 354–357, 2011.

[37] K. Han, J. Gil, S. -S. Song, J. Han, H. Shin, C. -K. Kim, and K. Lee, Complete high-frequency thermal noise modeling of short-channel MOSFETs and design of 5.2-GHz low noise amplifier, *IEEE Journal of Solid-State Circuits*, vol. 40, no. 3, pp. 726–735, 2005.

[38] S. Khaledian, F. Farzami, D. Erricolo, and B. Smida, A full-duplex bidirectional amplifier with low DC power consumption using tunnel diodes, *IEEE Microwave and Wireless Components Letters*, vol. 27, no. 12, pp. 1125–1127, 2017.